Monthly Notices of the ROYAL ASTRONOMICAL SOCIETY

MNRAS **442,** 1054–1067 (2014) doi:10.1093/mnras/stu928

Near-infrared counterparts of ultraluminous X-ray sources

M. Heida,[1,2]★ P. G. Jonker,[1,2,3] M. A. P. Torres,[1] E. Kool,[1] M. Servillat,[3,4] T. P. Roberts,[5] P. J. Groot,[2] D. J. Walton,[6] D.-S. Moon[7] and F. A. Harrison[6]

[1]*SRON Netherlands Institute for Space Research, Sorbonnelaan 2, NL-3584 CA Utrecht, the Netherlands*
[2]*Department of Astrophysics/IMAPP, Radboud University Nijmegen, PO Box 9010, NL-6500 GL Nijmegen, the Netherlands*
[3]*Harvard-Smithsonian Center for Astrophysics, 60 Garden Street, Cambridge, MA 02138, USA*
[4]*Laboratoire AIM (CEA/Irfu/SAp, CNRS/INSU, Université Paris Diderot), CEA Saclay, F-91191 Gif-sur-Yvette, France*
[5]*Department of Physics, University of Durham, South Road, Durham DH1 3LE, UK*
[6]*Space Radiation Laboratory, California Institute of Technology, Pasadena, CA 91125, USA*
[7]*Department of Astronomy and Astrophysics, University of Toronto, Toronto, ON M5S 3H4, Canada*

Accepted 2014 May 6. Received 2014 April 15; in original form 2014 March 4

ABSTRACT

In this paper, we present the results of the first systematic search for counterparts to nearby ultraluminous X-ray sources (ULXs) in the near-infrared (NIR). We observed 62 ULXs in 37 galaxies within 10 Mpc and discovered 17 candidate NIR counterparts. The detection of 17 out of 62 ULX candidates points to intrinsic differences between systems that show and those that do not show infrared emission. For six counterparts, we conclude from the absolute magnitudes and – in some cases – additional information such as morphology and previously reported photometric or spectroscopic observations, that they are likely background active galactic nuclei or ULXs residing in star clusters. 11 counterparts have absolute magnitudes consistent with them being single red supergiant stars. Alternatively, these systems may have larger accretion discs that emit more NIR light than the systems that we do not detect. Other scenarios such as emission from a surrounding nebula or from a compact radio jet are also possible, although for Holmberg II X-1 the NIR luminosity far exceeds the expected jet contribution. The 11 possible red supergiant counterparts are excellent candidates for spectroscopic follow-up observations. This may enable us to measure the mass function in these systems if they are indeed red supergiant donor stars where we can observe absorption lines.

Key words: stars: black holes – infrared: stars.

1 INTRODUCTION

Ultraluminous X-ray sources (ULXs) are point-like, off-nuclear X-ray sources with an X-ray luminosity above 10^{39} erg s^{-1} (Feng & Soria 2011), the Eddington luminosity of an $\sim$10 M$_\odot$ black hole. The most luminous example reaches 10^{42} erg s^{-1} (HLX-1, Farrell et al. 2009). Several scenarios have been proposed to explain the high luminosities of these sources. Geometrical beaming could boost the observed luminosity by up to a factor of $\sim$10 (King et al. 2001). Genuine super-Eddington accretion is another option (Begelman 2002; Moon, Eikenberry & Wasserman 2003). Alternatively, if these systems contain black holes that are more massive than 100 M$_\odot$ (which is our working definition of intermediate mass black holes, IMBHs), that would naturally explain the high luminosities.

Observations indicate that ULXs at lower and higher luminosity may belong to different populations. The luminosity functions of ULXs and fainter extragalactic X-ray binaries show a break around 2×10^{40} erg s^{-1} (Swartz et al. 2011; Mineo, Gilfanov & Sunyaev 2012). At luminosities below this break, the identification of an 'ultraluminous' X-ray spectral state (e.g. Gladstone, Roberts & Done 2009) added observational support to the idea that the majority of these ULXs are stellar-mass black holes accreting at super-Eddington rates, which are rarely observed in Galactic black hole X-ray binaries for reasons currently unknown. Alternatively, for a low-metallicity star it is possible to leave a black hole of $\lesssim$70 M$_\odot$ (Belczynski et al. 2010). Accretion on to such a black hole could explain ULXs with luminosities up to a few times 10^{40} erg s^{-1} (Zampieri & Roberts 2009). In this scenario, only the brightest ULXs, with X-ray luminosities $\gtrsim 2 \times 10^{40}$ erg s^{-1}, remain as plausible IMBH candidates. Such a seemingly convincing case for an IMBH is provided by the ULX ESO 243–49 X–1 (Farrell et al. 2009).

Ultimately, the most reliable way to determine the nature of ULXs is to obtain dynamical mass measurements of their black hole masses using radial velocity curves of their companion stars, as well as measurements of the system inclination and binary mass

★E-mail: m.heida@astro.ru.nl

© 2014 The Authors
Published by Oxford University Press on behalf of the Royal Astronomical Society

Downloaded from http://mnras.oxfordjournals.org/ at Durham University Library on July 8, 2014

ratio. Dynamical mass measurements of Galactic binary systems usually rely on optical spectroscopic observations of the motion of the companion star. Unfortunately, most attempts to use the same technique for ULXs have not met with success (cf. Roberts et al. 2011; Liu, Orosz & Bregman 2012; Cseh et al. 2013, however, see the recent work of Liu et al. 2013). The reason for this failure is that most optical counterparts to ULXs are faint, and, in the cases where it has been possible to perform spectroscopic studies, the spectra show strong emission lines from the accretion disc, the irradiated companion star and/or from the surrounding nebulae but no absorption features from a stellar component. The emission lines cannot be used for reliable dynamical mass measurements because their radial velocities vary erratically and on time-scales that may be unrelated to the orbital period of the system.

Searches for photospheric lines from the donor stars in ULXs have thus far concentrated on the blue part of the spectrum because ULX donor stars were expected to be blue supergiants. This expectation is based on the fact that many ULXs are located in or near young star clusters (e.g. Fabbiano, Zezas & Murray 2001; Roberts et al. 2002; Gao et al. 2003; Swartz, Tennant & Soria 2009; Voss et al. 2011) and on the blue colours of many ULX counterparts (e.g. Roberts et al. 2001; Liu, Bregman & Seitzer 2002). However, these blue colours are also consistent with emission from an irradiated accretion disc (Grisé et al. 2012; Soria et al. 2012). And if ULX donor stars are indeed massive young stars, some of them may very well be Wolf–Rayet stars (like the counterpart to M 101 ULX-1, Liu et al. 2013) or red supergiants (RSGs; Copperwheat et al. 2005, 2007; Patruno & Zampieri 2008).

Red supergiant (RSG) stars are intrinsically bright in the near-infrared (NIR) ($M_V \sim -6$, $V-H \sim 4$, $H-K \sim 0$) in contrast with the blue supergiants ($M_V \sim -6$, $V-H \sim 0$, $H-K \sim 0$; Elias, Frogel & Humphreys 1985; Drilling & Landolt 2000), and can outshine the accretion disc in that part of the spectrum. A Galactic analogue is GRS 1915−105, a black hole X-ray binary with a red giant companion star (not an RSG) with an orbital period of 33.5 d. A dynamical mass measurement of the black hole in this system was obtained from radial velocity studies in the NIR while the source was bright in X-rays, showing that irradiation of the companion star has little effect on long orbital period systems like this (Steeghs et al. 2013). A Roche lobe overflowing RSG would have an even larger orbit than the red giant in GRS 1915−105, so irradiation is not likely to produce strong effects in the companion atmosphere (Copperwheat et al. 2005, 2007). With the largest telescopes currently available, it is possible to perform time-resolved spectroscopy for sources with *H*- and *K*-band magnitudes up to ∼20. This corresponds to the typical apparent magnitude of an RSG at a distance of ∼10 megaparsec (Mpc).

In this paper, we present the results of our search for candidate RSG companions to ULXs within 10 Mpc. The sample consists of sources from several catalogues of ULX candidates. We describe the sample in Section 2, the observations in Section 3 and the data reduction in Section 4. The results, including a table summarizing all detected counterparts and limiting magnitudes for the non-detections, can be found in Section 5. In Section 6, we discuss our findings.

2 SAMPLE

Our sample consists mainly of ULX candidates from the catalogues of Swartz et al. (2004, 2011) and Walton et al. (2011), supplemented with additional targets from other sources (see Tables 1 and 2). We only targeted ULX candidates within a distance of 10 Mpc, since this is the maximum distance at which it is still viable to take an NIR spectrum of an RSG with existing large telescopes. ULX candidates in very crowded regions, such as edge-on spiral galaxies and fields close to galactic centres, were excluded from the sample.

Five candidates had no reported accurate X-ray positions when we started our observing campaign. For these sources, we determined an accurate X-ray position based on archival *Chandra*/Advanced CCD Imaging Spectrometer (ACIS) observations. We used the CIAO (Fruscione et al. 2006) task ACIS_PROCESS_EVENTS to reprocess the event files if the observations were conducted in very faint mode. Then we determined accurate positions for the ULX candidates using WAVDETECT. The sources and *Chandra* observation ID's are listed in Table 3. For the other sources, X-ray positions and uncertainties were taken from the literature (see Table 1). Quoted error radii on the source location are at the 95 per cent confidence level (2σ).

The complete sample consists of 62 ULX candidates in 37 galaxies. We have collected recent distance measurements for these galaxies where available to compute absolute magnitudes and absolute magnitude limits for the NIR counterparts, assuming they are at the same distance as their host galaxies (see Table 4). These are generally different from the distance measurements used to compile catalogues of ULX candidates. For example, Walton et al. (2011) use only distances from Tully (1988). Comparing these to the newer distance measurements showed that if there are significant differences, these older measurements generally underestimate the distance. Hence, the true X-ray luminosities of these sources only go up with the new distance measurements and all sources in our sample are still ULX candidates.

3 OBSERVATIONS

We obtained observations for this project using three different telescopes.[1] In the Northern hemisphere, we used the William Herschel Telescope with the Long-slit Intermediate Resolution Infrared Spectrograph (WHT/LIRIS) and the MMT with the SAO Wide-field InfraRed Camera (MMT/SWIRC) to obtain *H*- and/or *Ks*-band images of 51 and 16 sources, respectively. WHT/LIRIS provides a pixel scale of 0.25 arcsec pixel^{-1} and a field of view of 4.27 arcmin × 4.27 arcmin, MMT/SWIRC has a pixel scale of 0.15 arcsec pixel^{-1} and a field of view of 5.12 arcmin × 5.12 arcmin. For targets in the Southern hemisphere, we were granted 8 h of service mode observations with the Infrared Spectrometer And Array Camera on the Very Large Telescope (VLT/ISAAC, Moorwood et al. 1998) in period 89 (program 089.D-0663(A)) and 4 h in period 90 (program 090.D-0417(A)). This yielded *Ks*-band images of 14 sources in total. We observed the 10 sources in p89 in one observing block (OB) per source. For the four sources in p90, we used two (shorter) OBs per source; for two sources (in NGC 1637 and NGC 3621), these OBs were executed in the same night, whereas the OBs for the two ULXs in NGC 253 were executed 14 (J004722-252051) and 42 d (J004742-251501) apart, respectively. We used the SW imaging mode of ISAAC, which gives a spatial scale of 0.148 arcsec pixel^{-1} and a field of view of 152 arcsec × 152 arcsec.

All observations were performed using multiple repetitions of a 5-point dither pattern. We used exposure times of 20 s in the *H* band and 15 s in the *Ks* band with WHT/LIRIS and MMT/SWIRC, and exposure times of 6 or 10 s with VLT/ISAAC. The ULXs were not

[1] The data are publicly available at http://archive.eso.org and http://casu.ast.cam.ac.uk/casuadc/ingarch/.

Downloaded from http://mnras.oxfordjournals.org/ at Durham University Library on July 8, 2014

Table 1. The ULX candidates of which we obtained NIR images, with their designation from Simbad, their best determined X-ray position with the radius of the 95 per cent confidence error circle, and the catalogue ('this work' for sources for which we determined the position) and satellite that provided the position.

Galaxy	ULX name (SIMBAD)	RA (h:m:s)	Dec. (d:m:s)	Error	Source	Satellite
NGC 253	RX J004722.4−252051	00:47:22.59	−25:20:50.9	1.0 arcsec	Liu (2011)	*Chandra*
NGC 253	RX J004742.5−251501	00:47:42.76	−25:15:02.2	1.0 arcsec	Liu (2011)	*Chandra*
M74	[KKG2005] M74 X−1	01:36:51.06	15:45:46.8	0.7 arcsec	Liu (2011)	*Chandra*
M74	XMMU J013636.5+155036	01:36:36.5	15:50:36.3	0.8 arcsec	Lin, Webb & Barret (2012)	*XMM–Newton*
NGC 855	[SST2011] J021404.08+275239.5	02:14:04.09	27:52:39.4	1.0 arcsec	Liu (2011)	*Chandra*
NGC 925	[SST2011] J022721.52+333500.7	02:27:21.52	33:35:00.8	1.0 arcsec	Liu (2011)	*Chandra*
NGC 925	[SST2011] J022727.53+333443.0	02:27:27.53	33:34:42.9	1.0 arcsec	Liu (2011)	*Chandra*
NGC 1058	XMMU J024323.5+372038	02:43:23.27	37:20:42.1	0.7 arcsec	this work	*Chandra*
NGC 1313	RX J0318.3−6629	03:18:20.00	−66:29:10.9	1.0 arcsec	Liu (2011)	*Chandra*
IC342	XMMU J034555.6+680455	03:45:55.61	68:04:55.3	0.25 arcsec	Feng & Kaaret (2008)	*Chandra*
IC342	[SST2011] J034615.64+681112.2	03:46:15.61	68:11:12.8	0.4 arcsec	Lin et al. (2012)	*XMM–Newton*
NGC 1637	[IWL2003] 68	04:41:32.97	−02:51:26.8	1.0 arcsec	Liu (2011)	*Chandra*
NGC 2403	CXOU J073625.6+653539	07:36:25.55	65:35:40.0	0.7 arcsec	Swartz et al. (2004)	*Chandra*
NGC 2403	2E 0732.2+6546	07:37:02.33	65:39:35.0	0.7 arcsec	this work	*Chandra*
NGC 2500	[SST2011] J080148.10+504354.6	08:01:48.11	50:43:54.6	1.0 arcsec	Liu (2011)	*Chandra*
NGC 2500	CXO J080157.8+504339	08:01:57.84	50:43:39.4	1.0 arcsec	Liu (2011)	*Chandra*
Holmberg II	Holmberg II X−1	08:19:28.99	70:42:19.4	0.7 arcsec	Swartz et al. (2004)	*Chandra*
NGC 2903	CXOU J093206.2+213058	09:32:06.19	21:30:58.9	0.6 arcsec	Watson et al., in preparation	*XMM–Newton*
Holmberg I	[WMR2006] Ho I XMM1	09:41:30.15	71:12:35.7	1.0 arcsec	Watson et al., in preparation	*XMM–Newton*
Holmberg I	1WGA J0940.0+7106	09:39:59.44	71:06:40.2	1.0 arcsec	Watson et al., in preparation	*XMM–Newton*
Holmberg I	[WMR2006] Ho I XMM3	09:42:06.36	71:04:40.0	1.4 arcsec	Watson et al., in preparation	*XMM–Newton*
M81	[LM2005] NGC 3031 ULX1	09:55:32.95	69:00:33.6	1.0 arcsec	Liu (2011)	*Chandra*
Holmberg IX	Holmberg IX X−1	09:57:53.31	69:03:48.1	1.0 arcsec	Liu (2011)	*Chandra*
NGC 3184	CXOU J101812.0+412421	10:18:12.05	41:24:20.7	0.7 arcsec	Swartz et al. (2004)	*Chandra*
NGC 3239	[SST2011] J102506.98+170947.2	10:25:06.98	17:09:47.2	1.0 arcsec	Liu (2011)	*Chandra*
NGC 3239	[SST2011] J102508.20+170948.3	10:25:08.20	17:09:48.4	1.0 arcsec	Liu (2011)	*Chandra*
NGC 3486	XMMU J110022.4+285818	11:00:22.27	28:58:16.9	0.7 arcsec	this work	*Chandra*
NGC 3521	[SST2011] J110545.62+000016.2	11:05:45.63	00:00:16.5	1.0 arcsec	Liu (2011)	*Chandra*
NGC 3621	[GSE2009] B	11:18:15.16	−32:48:40.6	0.7 arcsec[a]	Gliozzi et al. (2009)	*Chandra*
NGC 3623	[LB2005] NGC 3623 ULX1	11:18:58.54	13:05:30.9	1.0 arcsec	Liu (2011)	*Chandra*
NGC 3627	[SST2011] J112020.90+125846.6	11:20:20.89	12:58:46.0	1.0 arcsec	Liu (2011)	*Chandra*
NGC 3627	[SST2011] J112018.32+125900.8	11:20:18.31	12:59:00.3	1.0 arcsec	Liu (2011)	*Chandra*
NGC 3628	CXOU J112037.3+133429	11:20:37.37	13:34:29.2	1.0 arcsec	Liu (2011)	*Chandra*
NGC 4136	CXOU J120922.6+295551	12:09:22.58	29:55:50.6	1.0 arcsec	Liu (2011)	*Chandra*
NGC 4136	[SST2011] J120922.18+295559.7	12:09:22.19	29:55:59.7	1.0 arcsec	Liu (2011)	*Chandra*
NGC 4204	[SST2011] J121510.91+203912.4	12:15:10.91	20:39:12.4	1.0 arcsec	Liu (2011)	*Chandra*
NGC 4258	RX J121844.0+471730	12:18:43.88	47:17:31.7	1.0 arcsec	Liu (2011)	*Chandra*
NGC 4258	RX J121857.7+471558	12:18:57.85	47:16:07.4	1.0 arcsec	Liu (2011)	*Chandra*
NGC 4258	[WMR2006] NGC4258 XMM1	12:18:47.66	47:20:54.7	0.8 arcsec	Watson et al., in preparation	*XMM–Newton*
NGC 4258	RX J121845.6+472420	12:18:45.51	47:24:20.2	1.0 arcsec	Watson et al., in preparation	*XMM–Newton*
NGC 4395	IXO 53	12:26:01.53	33:31:30.6	1.0 arcsec	Liu (2011)	*Chandra*
NGC 4449	RX J122818.0+440634	12:28:17.83	44:06:33.9	1.1 arcsec	Liu (2011)	*Chandra*
NGC 4559	RX J123551+27561	12:35:51.71	27:56:04.1	0.7 arcsec	Swartz et al. (2004)	*Chandra*
NGC 4618	[SST2011] J124129.14+410757.7	12:41:29.14	41:07:57.7	0.7 arcsec[a]	Swartz et al. (2011)	*Chandra*
NGC 5128	1RXH J132519.8−430312	13:25:19.87	−43:03:17.1	1.0 arcsec	Kraft et al. (2001)	*Chandra*
NGC 5128	CXOU J132518.2−430304	13:25:18.24	−43:03:04.5	0.4 arcsec	Sivakoff et al. (2008)	*Chandra*
NGC 5204	CXOU J132938.6+582506	13:29:38.62	58:25:05.6	1.0 arcsec	Liu (2011)	*Chandra*
M51	RX J132943+47115	13:29:43.31	47:11:34.8	0.7 arcsec	Terashima, Inoue & Wilson (2006)	*Chandra*
M51	XMMU J132950.7+471153	13:29:50.68	47:11:55.2	0.7 arcsec	Terashima et al. (2006)	*Chandra*
M51	XMMU J132953.3+471040	13:29:53.31	47:10:42.5	0.7 arcsec	Terashima et al. (2006)	*Chandra*
M51	RX J132954+47145	13:29:53.72	47:14:35.7	0.7 arcsec	Terashima et al. (2006)	*Chandra*
M51	XMMU J132957.6+471047	13:29:57.57	47:10:48.3	0.7 arcsec	Terashima & Wilson (2004)	*Chandra*
M51	RX J133001+47137	13:30:01.01	47:13:43.9	0.7 arcsec	Terashima et al. (2006)	*Chandra*
M51	RX J133006+47156	13:30:06.00	47:15:42.3	0.7 arcsec	Terashima et al. (2006)	*Chandra*
M51	RX J133007+47110	13:30:07.55	47:11:06.1	0.7 arcsec	Terashima et al. (2006)	*Chandra*
NGC 5408	NGC 5408 X−1	14:03:19.63	−41:22:58.7	1.2 arcsec	Kaaret et al. (2003)	*Chandra*
NGC 5474	NGC 5474−X1	14:04:59.74	53:38:09.0	1.0 arcsec	Liu (2011)	*Chandra*
M101	CXOU J140332.3+542103	14:03:32.38	54:21:03.0	0.7 arcsec	Swartz et al. (2004)	*Chandra*
M101	2E 1402.4+5440	14:04:14.28	54:26:03.6	0.7 arcsec	Swartz et al. (2004)	*Chandra*
M101	2XMM J140248.0+541350	14:02:48.19	54:13:50.7	0.7 arcsec	this work	*Chandra*
M101	CXOU J140314.3+541807	14:03:14.33	54:18:06.7	0.7 arcsec	this work	*Chandra*
NGC 5585	[SST2011] J141939.39+564137.8	14:19:39.39	56:41:37.8	1.0 arcsec	Liu (2011)	*Chandra*

Notes. [a]No positional error was given in the cited article, we assume the standard *Chandra* bore-sight error of 0.6 arcsec (90 per cent confidence) and a localization error of less than 0.1 arcsec (90 per cent confidence), which combine into an 0.7 arcsec total error (95 per cent confidence).

Downloaded from http://mnras.oxfordjournals.org/ at Durham University Library on July 8, 2014

Table 2. Entries (marked with •) and/or names of our sources in other catalogues. Sources are listed in the same order as in Table 1. (1): Swartz et al. (2004), (2): Liu & Bregman (2005), (3): Liu & Mirabel (2005), (4): Winter, Mushotzky & Reynolds (2006), (5): Walton et al. (2011),(6): Swartz et al. (2011), (7): Barnard (2010).

ULX name (short)	(1)	(2)	(3)	(4)	(5)	(6)	Other
J004722−252051		NGC 253 X9		NGC 253 XMM2	•		NGC 253 ULX1[7]
J004742−251501		NGC 253 X6		NGC 253 XMM6			NGC 253 ULX3[7]
M74 X-1	•		NGC 628 ULX1		•		CXOU J013651.1+154547
J013636+155036			NGC 628 ULX2		•		
J021404+275239						•	CXOU J021404.0+275239
J022721+333500						•	CXOU J022721.5+333500
J022727+333443						•	CXOU J022727.5+333442
J024323+372038			NGC 1058 ULX1		•		CXOU J024323.2+372042
J0318−6629		NGC 1313 X2	NGC 1313 ULX1	NGC 1313 XMM1	•		CXOU J031820.0−662911
J034555+680455		PGC13826 X6	IC 342 ULX1	IC 342 XMM1	•	•	IC 342 X-1
J034615+681112		PGC13826 X7			•	•	2XMM J034615.6+681112
[IWL2003] 68							CXOU J044132.9−025126
J073625+653539	•	NGC 2403 X2	NGC 2403 ULX1	NGC 2403 XMM1	•	•	
J0732+6546		NGC 2403 X3		NGC 2403 XMM4	•		CXOU J073702.3+653935
J080148+504354						•	CXOU J080148.1+504354
J080157+504339						•	
Holmberg II X-1	•	PGC 23324 ULX1	Holmberg II ULX1	Ho II XMM1	•	•	
J093206+213058						•	3XMM J093206.1+213058
Ho I XMM1				Ho I XMM1			3XMM J094130.1+711235
J0940+7106				Ho I XMM2			3XMM J093959.4+710640
Ho I XMM3				Ho I XMM3			3XMM J094206.3+710444
NGC 3031 ULX1	•		NGC 3031 ULX1	M81 XMM1		•	CXOU J095532.9+690033
Holmberg IX X-1		PGC 28757 X2	NGC 3031 ULX2	Ho IX XMM1			CXOU J095753.3+690348
J101812+412421	•					•	
J102506+170947						•	CXOU J102506.9+170947
J102508+170948						•	CXOU J102508.2+170948
J110022+285818					•		CXOU J110021.7+285818
J110545+000016					•		CXOU J110545.6+000016
NGC3621 B							
NGC 3623 ULX1		NGC 3623 X2			•	•	CXOU J111858.5+130530
J112020+125846		NGC 3627 X2			•	•	CXOU J112020.8+125846
J112018+125900						•	CXOU J112018.3+125900
J112037+133429		NGC 3628 X2	NGC 3628 ULX2			•	
J120922+295551		NGC 4136 X1	NGC 4136 ULX1				
J120922+295559			NGC 4136 ULX2			•	CXOU J120922.1+29555
J121510+203912						•	CXOU J121510.9+203912
J121844+471730	•				•	•	CXOU J121843.8+471731
J121857+471558	•		NGC 4258 X3	NGC4258 XMM2	•	•	CXOU J121857.8+471607
NGC4258 XMM1				NGC4258 XMM1	•		3XMM J121847.6+472054
J121845+472420					•		3XMM J121845.5+472420
IXO 53		NGC 4395 X1	NGC 4395 ULX1	NGC4395 XMM1		•	CXOU J122601.5+333130
J122818+440634	•	NGC 4449 X5		NGC4449 XMM1		•	CXOU J122817.8+440633
J123551+27561	•	NGC 4559 X5	NGC 4559 ULX1		•	•	CXOU J123551.7+275604
J124129+410757						•	
J132519−430312		NGC 5128 X4	NGC 5128 ULX1				CXOU J132519.9−430317
J132518−430304							
J132938+582506	•	NGC 5204 X1	NGC 5204 ULX1	NGC5204 XMM1	•	•	
J132943+47115	•	NGC 5194 X4	NGC 5194−5 ULX2			•	
J132950+471153	•		NGC 5194−5 ULX3			•	
J132953+471040	•		NGC 5194−5 ULX4		•	•	
J132954+47145	•	NGC 5194 X9	NGC 5194−5 ULX5	M51 XMM7		•	CXOM51 J132953.7+471436
J132957+471047	•			M51 XMM6		•	
J133001+47137		NGC 5194 X6	NGC 5194−5 ULX7	M51 XMM3	•	•	
J133006+47156		NGC 5195 X2	NGC 5194−5 ULX9	M51 XMM4	•	•	
J133007+47110	•	NGC 5194 X8	NGC 5194−5 ULX8	M51 XMM2	•	•	CXOM51 J133007.6+471106
NGC 5408 X-1			NGC 5408 ULX1	NGC5408 XMM1	•		
NGC 5474 X-1						•	CXOU J140459.7+533808
J140332+542103	•	NGC 5457 X5	NGC 5457 ULX7			•	
J1402+5440	•	NGC 5457 X23	NGC 5457 ULX3	M101 XMM3	•	•	CXOU J140414.3+542604
J140248+541350					•		CXOU J140248.1+541350
J140314+541807			NGC 5457 ULX2	M101 XMM1	•		
J141939+564137						•	CXOU J141939.3+564137

Downloaded from http://mnras.oxfordjournals.org/ at Durham University Library on July 8, 2014

Table 3. The ULX candidates for which we calculated accurate X-ray positions from archival *Chandra* observations.

ULX candidate	*Chandra* obs. ID
J024323+372038	9579
J0732+6546	2014
J110022+285818	393
J140248+541350	14341
J140314+541807	14341

necessarily centred on the detectors as the pointings were selected to minimize the background from the galaxy, maximize the number of reference stars in the field and avoid very bright stars. However, if the host galaxy covered more than half of the field of view of the image, we alternated between the target and an off-target blank sky field to properly subtract the sky background.

A log of the observations including the total exposure time for each source, the size of the point spread function in the image as a measure of the image quality, the distance modulus to the galaxy and the uncertainty in the astrometry is shown in Table 4.

Table 4. Log of the observations, with the distance modulus to the assumed host galaxy of the ULX candidates. The image number can be used to link details of the observations to the data on individual ULXs in Table 5. I.Q. is the image quality. The last column gives the 1σ uncertainty in the astrometry of the image.

Im. no.	Galaxy	Filter	Instrument/ Telescope	Obs. date	Exp. time (s)	I.Q. (arcsec)	Distance modulus (mag)	WCS uncertainty[a] (arcsec)
1	NGC 253	*Ks*	ISAAC/VLT	2012-11-19[b]	750	0.7	27.7 ± 0.1[1]	0.26
2	NGC 253	*Ks*	ISAAC/VLT	2012-11-19[b]	750	0.4	27.7 ± 0.1[1]	0.48
3	M74	*Ks*	ISAAC/VLT	2012-07-06	260	1.0	30.0 ± 0.4[5]	0.5[d]
4	M74	*Ks*	LIRIS/WHT	2012-01-01	7125	0.8	30.0 ± 0.4[5]	0.36
5	M74	*H*	LIRIS/WHT	2013-01-29	3860	0.5	30.0 ± 0.4[5]	0.64
6	M74	*Ks*	LIRIS/WHT	2012-01-04	9105	0.7	30.0 ± 0.4[5]	0.14
7	NGC 855	*Ks*	LIRIS/WHT	2012-01-05	4350	0.8	29.94 ± 0.17[18]	0.33
8	NGC 925	*Ks*	LIRIS/WHT	2012-01-01	9285	0.7	29.3 ± 0.4[9]	0.17
9	NGC 925	*H*	LIRIS/WHT	2013-01-29	3000	0.6	29.3 ± 0.4[9]	0.28
10	NGC 1058	*Ks*	LIRIS/WHT	2012-01-05	5625	0.6	29.8 ± 0.4[7]	0.24
11	NGC 1058	*H*	LIRIS/WHT	2013-01-29	3000	1.0	29.8 ± 0.4[7]	0.27
12	NGC 1313	*Ks*	ISAAC/VLT	2012-07-05	160	0.6	28.2 ± 0.2[8]	0.42
13	IC342	*Ks*	LIRIS/WHT	2012-01-04	7410	0.8	27.72 ± 0.17[2]	0.21
14	IC342	*Ks*	LIRIS/WHT	2012-01-01	3975	1.7	27.72 ± 0.17[2]	0.22
15	IC342	*H*	LIRIS/WHT	2013-01-27	4000	0.9	27.72 ± 0.17[2]	0.23
16	NGC 1637	*Ks*	ISAAC/VLT	2012-11-22	750	0.3	30.0 ± 0.4[9]	0.4
17	NGC 2403	*Ks*	LIRIS/WHT	2012-01-01	6345	2.3	27.50 ± 0.05[8]	0.28
18	NGC 2403	*H*	LIRIS/WHT	2013-01-26	4000	0.7	27.50 ± 0.05[8]	0.29
19	NGC 2403	*Ks*	LIRIS/WHT	2012-01-04	7500	1.6	27.50 ± 0.05[8]	0.28
20	NGC 2500	*Ks*	LIRIS/WHT	2012-01-01	5580	1.5	30.0 ± 0.4[7]	0.06
21	NGC 2500	*Ks*	LIRIS/WHT	2012-01-07	6855	0.6	30.0 ± 0.4[7]	0.12
22	Holmberg II	*Ks*	LIRIS/WHT	2012-01-05	3750	0.9	27.65 ± 0.03[1]	0.22
23	Holmberg II	*Ks*	LIRIS/WHT	2013-01-27	3675	1.0	27.65 ± 0.03[1]	0.39
24	Holmberg II	*H*	SWIRC/MMT	2011-05-17	1120	0.5	27.65 ± 0.03[1]	0.23
25	NGC 2903	*H*	LIRIS/WHT	2013-01-29	3940	1.0	30.1 ± 0.4[10]	0.13
26	Holmberg I	*H*	SWIRC/MMT	2011-05-17	900	0.8	27.95 ± 0.03[1]	0.14
27	Holmberg I	*H*	SWIRC/MMT	2011-05-17	900	0.8	27.95 ± 0.03[1]	0.17
28	Holmberg I	*H*	SWIRC/MMT	2011-05-17	600	1.0	27.95 ± 0.03[1]	0.14
29	M81	*Ks*	LIRIS/WHT	2012-01-08	3375	0.9	27.86 ± 0.06[6]	0.12
30	Holmberg IX	*H*	SWIRC/MMT	2011-05-17	1200	1.0	27.79 ± 0.08[1]	0.25
31	NGC 3184	*Ks*	LIRIS/WHT	2012-01-07	3780	1.0	30.5 ± 0.5[5]	0.47[c]
32	NGC 3239	*Ks*	LIRIS/WHT	2012-01-01	2085	1.7	29.5 ± 0.4[7]	0.55
33	NGC 3239	*H*	LIRIS/WHT	2013-01-25	3820	0.7	29.5 ± 0.4[7]	0.39
34	NGC 3486	*Ks*	LIRIS/WHT	2012-01-07	1695	0.7	31.1 ± 0.4[11]	0.30
35	NGC 3521	*Ks*	ISAAC/VLT	2012-05-16	120	0.7	31.1 ± 0.4[10]	0.5[d]
36	NGC 3621	*Ks*	ISAAC/VLT	2013-01-01	750	0.4	28.9 ± 0.4[9]	0.23
37	NGC 3623	*Ks*	ISAAC/VLT	2012-06-09	120	0.6	30.5 ± 0.4[10]	0.14
38	NGC 3627	*Ks*	ISAAC/VLT	2012-06-10	120	0.7	29.7 ± 0.4[9]	0.24
39	NGC 3628	*Ks*	ISAAC/VLT	2012-06-10	120	0.9	30.7 ± 0.5[12]	0.50[c]
40	NGC 4136	*H*	LIRIS/WHT	2013-01-25	3980	0.9	29.9 ± 0.4[7]	0.34
41	NGC 4204	*H*	LIRIS/WHT	2013-01-29	2940	1.0	29.5 ± 0.4[7]	0.62[c]
42	NGC 4258	*H*	LIRIS/WHT	2013-01-27	5000	0.8	29.29 ± 0.02[13]	0.5[d]
43	NGC 4258	*H*	LIRIS/WHT	2013-01-27	4000	0.7	29.29 ± 0.02[13]	0.31
44	NGC 4258	*H*	LIRIS/WHT	2013-01-27	4000	0.7	29.29 ± 0.02[13]	0.27
45	NGC 4395	*Ks*	LIRIS/WHT	2012-01-04	5595	1.2	28.42 ± 0.02[8]	0.32
46	NGC 4449	*Ks*	LIRIS/WHT	2012-01-04	3435	0.9	28.0 ± 0.1[14]	0.35
47	NGC 4559	*H*	LIRIS/WHT	2013-01-25	3400	0.8	29.6 ± 0.5[10]	0.28
48	NGC 4559	*H*	SWIRC/MMT	2011-05-17	6680	0.8	29.6 ± 0.5[10]	0.12

Downloaded from http://mnras.oxfordjournals.org/ at Durham University Library on July 8, 2014

Table 4 – *continued*

Im. no.	Galaxy	Filter	Instrument/ Telescope	Obs. date	Exp. time (s)	I.Q. (arcsec)	Distance modulus (mag)	WCS uncertainty[a] (arcsec)
49	NGC 4618	*Ks*	LIRIS/WHT	2012-01-07	5265	0.9	29.3 ± 0.4[7]	0.62
50	NGC 5128	*Ks*	ISAAC/VLT	2012-04-22	120	0.3	27.77 ± 0.17[15]	0.16
51	NGC 5204	*Ks*	LIRIS/WHT	2011-05-16	5040	1.0	28.3 ± 0.3[16]	0.10
52	M51	*H*	LIRIS/WHT	2013-01-29	3460	1.2	29.6 ± 0.2[4]	0.28
53	M51	*H*	LIRIS/WHT	2013-01-29	3140	1.3	29.6 ± 0.2[4]	0.35
54	M51	*H*	LIRIS/WHT	2013-01-29	3500	1.5	29.6 ± 0.2[4]	0.23
55	NGC 5408	*Ks*	ISAAC/VLT	2012-04-22	120	0.3	28.4 ± 0.8[7]	0.26
56	NGC 5474	*Ks*	LIRIS/WHT	2012-01-05	4935	1.2	29.15[17]	0.46[c]
57	M101	*H*	SWIRC/MMT	2011-05-17	1160	1.2	29.04 ± 0.05[3]	0.36
58	M101	*H*	SWIRC/MMT	2011-05-17	1200	0.7	29.04 ± 0.05[3]	0.23
59	M101	*H*	SWIRC/MMT	2011-05-17	1200	0.7	29.04 ± 0.05[3]	0.15
60	M101	*H*	SWIRC/MMT	2011-05-17	1180	0.9	29.04 ± 0.05[3]	0.12
61	NGC 5585	*Ks*	LIRIS/WHT	2012-01-05	4950	1.1	29.9 ± 0.6[10]	0.06

Notes. [a] rms error with respect to the reference catalogue. The 2MASS catalogue was used for the astrometric calibration, unless stated otherwise. [b]Date of the first observation. The second observations were taken on 2012-12-03 (#1) and 2012-12-31 (#2). [c]USNO B1.0 catalogue used for astrometric calibration. [d]Less than four sources available for astrometric calibration. [1]Dalcanton et al. (2009), [2]Herrmann et al. (2008), [3]Shappee & Stanek (2011), [4]Poznanski et al. (2009), [5]Olivares E. et al. (2010), [6]Durrell, Sarajedini & Chandar (2010), [7]Tully (1988), [8]Jacobs et al. (2009), [9]Tully et al. (2009), [10]Springob et al. (2009), [11]Theureau et al. (2007), [12]Willick et al. (1997), [13]Humphreys et al. (2008), [14]McQuinn et al. (2010), [15]Chattopadhyay et al. (2009), [16]Karachentsev et al. (2003), [17]Drozdovsky & Karachentsev (2000), [18]Tonry et al. (2001).

4 DATA REDUCTION AND ANALYSIS

The data obtained with VLT/ISAAC in period 89 were reduced with the ISAAC pipeline in the GASGANO environment, following the steps outlined in the ISAAC Data Reduction Guide.[2] The output of the pipeline is a co-added, sky-subtracted image without astrometric calibration. We used the astrometry tool 'fit to star positions' in the STARLINK program GAIA to calculate the astrometric solutions, using 2 Micron All Sky Survey (2MASS; Skrutskie et al. 2006) sources in the field of view if at least four were present. When this was not the case, we used sources from the USNO B1.0 catalogue (Monet et al. 2003) for the calibration. We adopt the root-mean-square (rms) error of the fit as the 1σ uncertainty on the positions of the NIR sources. We used the general data-reduction software package THELI (Schirmer 2013) to reduce the data obtained with WHT/LIRIS, MMT/SWIRC and the data obtained with VLT/ISAAC in p90. The greater flexibility of THELI makes it easier to immediately combine data taken on different nights, hence we decided to use it instead of the ISAAC pipeline for the reduction of the VLT/ISAAC data from p90. Because the final astrometric and photometric calibration was done in a uniform way for all images, we are confident that the use of different data-reduction packages does not impact our results. Using THELI, we first produced master flats, applied them to the images and subtracted the sky background of the individual frames. THELI employs SEXTRACTOR (Bertin & Arnouts 1996) and SCAMP (Bertin 2006) to find sources in the individual images and determine an astrometric solution by matching their positions to sources from 2MASS or PPXML (Roeser, Demleitner & Schilbach 2010) if not enough 2MASS sources are present. This astrometric solution is then used to co-add the images using SWARP (Bertin et al. 2002). We improved the astrometric accuracy of the final co-added images using the 'fit to star positions' tool in GAIA, again fitting to positions of sources from 2MASS or USNO B1.0. The rms errors on these fits are listed in Table 4 as a measure of the uncertainty in the astrometry of the NIR images. Three images (#20, 45 and 52) did not have a sufficient number of 2MASS or USNO B1.0 sources in the field of view. We calibrated these images using only three reference stars from 2MASS. With three reference stars and three degrees of freedom no rms error could be calculated. For these images, we adopt a 1σ uncertainty of 0.5 arcsec.

We calculated the radius of the 95 per cent confidence (2σ) error circle around the position of the ULX candidates on the NIR images by quadratically adding the 2σ uncertainty on the X-ray position and twice the rms error of the astrometric solution of the NIR images. There is an additional uncertainty in the 2MASS and USNO B1.0 positions with respect to the international celestial reference system, but this error (0.015 arcsec for 2MASS, 0.2 arcsec for USNO B1.0, Skrutskie et al. 2006; Monet et al. 2003) is negligible in the total error budget (that is dominated by the uncertainty in the X-ray position).

We used the tasks DAOFIND and PHOT from the APPHOT package in IRAF[3] to calibrate the zero-points of the images using 2MASS sources near the targets, detect counterparts within the error circles and calculate their apparent magnitude. For the cases where we did not detect a counterpart, we calculated the limiting magnitude at the position of the ULX by simulating stars at that position with a range of magnitudes using the IRAF task MKOBJECTS. The magnitude of the faintest simulated star that was still detected at the three sigma level was taken as a robust lower limit for the magnitude of the ULX.

5 RESULTS

Of the 62 ULX candidates in our sample, 17 have a candidate counterpart in one or more NIR images. The apparent and absolute magnitudes of the candidate counterparts are listed in Table 5.

[2] ftp.eso.org/pub/dfs/pipelines/isaac/isaac-pipeline-manual-1.4.pdf

[3] IRAF is distributed by the National Optical Astronomy Observatory, which is operated by the Association of Universities for Research in Astronomy under cooperative agreement with the National Science Foundation.

Downloaded from http://mnras.oxfordjournals.org/ at Durham University Library on July 8, 2014

If a ULX has no detected counterpart, the limiting magnitude of the image at the position of the ULX is given. The errors on the apparent magnitudes reported in Table 5 are the 1σ errors on the magnitude determination by IRAF and on the zero-point calibration. For the absolute magnitudes, there is an additional error that stems from the uncertainty in the distance modulus (listed in Table 4).

5.1 NIR counterparts

We detected candidate counterparts for 17 ULX candidates in our sample. Because some of these have been observed more than once, the total number of detections is 23. There are 11 sources in the *Ks* band and 12 in the *H* band. The absolute magnitudes of the candidate counterparts range from −7.1 to −13.88 in the *H* band and from −8.1 to −14.3 in the *Ks* band, with the majority of the sources lying between −9 and −11.5 in both bands (see Table 5).

5.2 Limiting magnitudes for non-detections

For the remaining 45 ULX candidates in our sample, we only have lower limits on their NIR magnitudes, 29 in the *Ks* band and 23 in the *H* band. The apparent limiting magnitudes range from 17 to 21.25 in both NIR bands. Our aim was to reach a limiting magnitude of at least 20. Worse limits are mainly caused by bad seeing (although most of the sources that were observed under bad seeing conditions were subsequently repeated under better conditions) and crowding or high backgrounds from the host galaxies, especially in e.g. the spiral arms of M101 and M51.

The absolute limiting magnitudes vary from −7.5 to −12 in the *Ks* band and from −7.5 to −12.6 in the *H* band.

Table 5. Apparent and absolute magnitudes of the candidate NIR counterparts to the ULX candidates, or upper limits for ULXs where we did not detect a source in the error circle around the X-ray position. The image number refers to the observation log (Table 4). The error radius is the radius of the 95 per cent confidence circle around the position of the ULX within which we search for counterparts. It is derived by quadratically adding the positional error on the location of the X-ray sources and two times the rms error of the astrometric solution of fitting stellar positions on the NIR images.

Galaxy	ULX name	Im. no.	Error Radius	Det. y/n	Filter	Apparent magnitude[a]	Absolute magnitude[a]
NGC 253	J004722−252051	1	1.1 arcsec	y	*Ks*	$17.2 \pm 0.03 \pm 0.5$	$-10.5 \pm 0.03 \pm 0.5 \pm 0.10$
NGC 253	J004742−251501	2	1.4 arcsec	n	*Ks*	>19.5	>−8.2
M74	M74 X-1	3	1.2 arcsec	n	*Ks*	>20.0	>−10.0
		4	1.0 arcsec	n	*Ks*	>20.0	>−10.0
		5	1.5 arcsec	n	*H*	>21.25	>−8.8
M74	J013636+155036	6	0.8 arcsec	n	*Ks*	>21.25	>−8.8
NGC 855	J021404+275239	7	1.2 arcsec	n	*Ks*	>18.25	>−11.7
NGC 925	J022721+333500	8	1.1 arcsec	y	*Ks*	$18.0 \pm 0.03 \pm 0.2$	$-11.3 \pm 0.03 \pm 0.2 \pm 0.4$
		9	1.1 arcsec	y	*H*	$18.7 \pm 0.03 \pm 0.2$	$-10.6 \pm 0.03 \pm 0.2 \pm 0.4$
NGC 925	J022727+333443	8	1.1 arcsec	y	*Ks*	$19.5 \pm 0.08 \pm 0.2$	$-9.8 \pm 0.08 \pm 0.2 \pm 0.4$
		9	1.1 arcsec	y	*H*	$20.1 \pm 0.08 \pm 0.2$	$-9.2 \pm 0.08 \pm 0.2 \pm 0.4$
NGC 1058	J024323+372038	10	0.8 arcsec	y	*Ks*	$19.7 \pm 0.06 \pm 0.4$	$-10.1 \pm 0.06 \pm 0.4 \pm 0.4$
		11	0.9 arcsec	y	*H*	$20.8 \pm 0.2 \pm 0.3$	$-9.0 \pm 0.2 \pm 0.3 \pm 0.4$
NGC 1313	J0318−6629	12	1.3 arcsec	n	*Ks*	>18.5	>−9.7
IC342	J034555+680455	13	0.5 arcsec	n	*Ks*	>20.25	>−7.5
IC342	J034615+681112	14	0.6 arcsec	n	*Ks*	>18.5	>−9.2
		15	0.6 arcsec	n	*H*	>20.0	>−7.7
NGC 1637	[IWL2003] 68	16	1.3 arcsec	y	*Ks*	$16.3 \pm 0.005 \pm 0.5$	$-13.7 \pm 0.005 \pm 0.5 \pm 0.4$
NGC 2403	J073625+653539	17	0.9 arcsec	n	*Ks*	>18.25	>−9.3
		18	0.9 arcsec	n	*H*	>20.0	>−7.5
NGC 2403	J0732+6546	19	0.9 arcsec	n	*Ks*	>19.25	>−8.3
NGC 2500	J080148+504354	20	1.0 arcsec	n	*Ks*	>19.75	>−10.3
NGC 2500	J080157+504339	20	1.0 arcsec	y	*Ks*	$15.7 \pm 0.002 \pm 0.2$	$-14.3 \pm 0.002 \pm 0.2 \pm 0.4$
		21	1.0 arcsec	y	*Ks*	$15.95 \pm 0.005 \pm 0.15$	$-14.1 \pm 0.005 \pm 0.15 \pm 0.4$
Holmberg II	Holmberg II X-1	22	0.8 arcsec	y	*Ks*	$19.30 \pm 0.08 \pm 0.10$	$-8.35 \pm 0.08 \pm 0.10 \pm 0.03$
		23	1.0 arcsec	y	*Ks*	$19.4 \pm 0.12 \pm 0.2$	$-8.2 \pm 0.12 \pm 0.2 \pm 0.03$
		24	0.8 arcsec	y	*H*	$20.6 \pm 0.3 \pm 0.10$	$-7.1 \pm 0.3 \pm 0.10 \pm 0.03$
NGC 2903	J093206+213058	25	0.7 arcsec	n	*H*	>20.25	>−9.9
Holmberg I	Ho I XMM1	26	1.0 arcsec	y	*H*	$17.81 \pm 0.01 \pm 0.10$	$-10.14 \pm 0.01 \pm 0.10 \pm 0.03$
Holmberg I	J0940+7106	27	1.1 arcsec	n	*H*	>19.25	>−8.7
Holmberg I	Ho I XMM3	28	1.4 arcsec	n	*H*	>20.5	>−9.6
M81	NGC 3031 ULX1	29	1.0 arcsec	n	*Ks*	>18.5	>−9.4
Holmberg IX	Holmberg IX X-1	30	1.2 arcsec	n	*H*	>19.75	>−8.0
NGC 3184	J101812+412421	31	1.2 arcsec	n	*Ks*	>20.5	>−10.0
NGC 3239	J102506+170947	32	1.5 arcsec	n	*Ks*	>18.25	>−11.3
		33	1.3 arcsec	n	*H*	>20.25	>−9.3
NGC 3239	J102508+170948	32	1.5 arcsec	n	*Ks*	>17.5	>−12.0
		33	1.3 arcsec	n	*H*	>20.25	>−9.3
NGC 3486	J110022+285818	34	0.9 arcsec	n	*Ks*	>20.0	>−11.1
NGC 3521	J110545+000016	35	1.4 arcsec	n	*Ks*	>19.25	>−11.9

Downloaded from http://mnras.oxfordjournals.org/ at Durham University Library on July 8, 2014

Table 5 *–continued*

Galaxy	ULX	Im. no.	Error Radius	Det. y/n	Filter	Apparent magnitude	Absolute magnitude
NGC 3621	NGC3621 B	36	0.8 arcsec	n	*Ks*	>18.0	>−10.9
NGC 3623	NGC 3623 ULX1	37	1.0 arcsec	n	*Ks*	>19.75	>−10.8
NGC 3627	J112020+125846	38	1.1 arcsec	n	*Ks*	>20.0	>−9.7
NGC 3627	J112018+125900	38	1.1 arcsec	y	*Ks*	$20.6 \pm 1.9 \pm 0.7$	$-9.1 \pm 1.9 \pm 0.7 \pm 0.4$
NGC 3628	J112037+133429	39	1.4 arcsec	n	*Ks*	>19.5	>−11.2
NGC 4136	J120922+295551	40	1.2 arcsec	y	*H*	$19.13 \pm 0.03 \pm 0.10$	$-10.78 \pm 0.03 \pm 0.10 \pm 0.4$
NGC 4136	J120922+295559	40	1.2 arcsec	y	*H*	$19.15 \pm 0.03 \pm 0.10$	$-10.75 \pm 0.03 \pm 0.10 \pm 0.4$
NGC 4204	J121510+203912	41	1.6 arcsec	n	*H*	>20.25	>−9.3
NGC 4258	J121844+471730	42	1.4 arcsec	n	*H*	$17.79 \pm 0.02 \pm 0.10$	$-11.50 \pm 0.02 \pm 0.1 \pm 0.02$
NGC 4258	J121857+471558	43	1.2 arcsec	n	*H*	>19.0	>−10.3
NGC 4258	NGC4258 XMM1	42	1.3 arcsec	n	*H*	>19.5	>−9.8
NGC 4258	J121845+472420	44	1.1 arcsec	n	*H*	>21.0	>−8.3
NGC 4395	IXO 53	45	1.2 arcsec	n	*Ks*	>20.0	>−8.4
NGC 4449	J122818+440634	46	1.3 arcsec	n	*Ks*	>18.25	>−9.8
NGC 4559	J123551+27561	47	0.9 arcsec	n	*H*	>21.0	>−8.6
		48	0.7 arcsec	n	*H*	>21.25	>−8.4
NGC 4618	J124129+410757	49	1.4 arcsec	n	*Ks*	>20.25	>−9.1
NGC 5128	J132519−430312	50	1.0 arcsec	n	*Ks*	>18.5	>−9.3
NGC 5128	J132518−430304	50	0.5 arcsec	n	*Ks*	>19.25	>−8.5
NGC 5204	J132938+582506	51	1.0 arcsec	n	*Ks*	>19.0	>−9.3
M51	J132943+47115	52	0.9 arcsec	n	*H*	>17.5	>−12.1
M51	J132950+471153	52	0.9 arcsec	n	*H*	>17.25	>−12.4
M51	J132953+471040	52	0.9 arcsec	y	*H*	$15.72 \pm 0.02 \pm 0.10$	$-13.88 \pm 0.02 \pm 0.10 \pm 0.2$
M51	J132954+47145	53	1.0 arcsec	n	*H*	>20.5	>−9.1
M51	J132957+471047	52	0.9 arcsec	n	*H*	>17.5	>−12.1
M51	J133001+47137	52	0.9 arcsec	n	*H*	>17.0	>−12.6
M51	J133006+47156	53	1.0 arcsec	n	*H*	>18.5	>−11.1
M51	J133007+47110	54	0.8 arcsec	n	*H*	>19.5	>−10.1
NGC 5408	NGC 5408 X-1	55	1.3 arcsec	y	*Ks*	$20.3 \pm 0.13 \pm 0.2$	$-8.1 \pm 0.13 \pm 0.2 \pm 0.8$
NGC 5474	NGC 5474-X1	56	1.4 arcsec	n	*Ks*	>19.5	>−9.7
M101	J140332+542103	57	1.0 arcsec	n	*H*	>18.5	>−10.5
M101	J1402+5440	58	0.8 arcsec	y	*H*	$19.3 \pm 0.04 \pm 0.2$	$-9.7 \pm 0.04 \pm 0.2 \pm 0.05$
M101	J140248+541350	59	0.8 arcsec	y	*H*	$17.72 \pm 0.01 \pm 0.05$	$-11.32 \pm 0.01 \pm 0.05 \pm 0.05$
M101	J140314+541807	60	0.7 arcsec	y	*H*	$18.35 \pm 0.03 \pm 0.10$	$-10.69 \pm 0.03 \pm 0.10 \pm 0.05$
NGC 5585	J141939+564137	61	1.0 arcsec	n	*Ks*	>19.75	>−10.2

Notes. [a]Magnitude and errors are as follows. Apparent/absolute magnitude ± statistical error on the magnitude as given by the PHOT routine ± statistical error on the zero-point of the image ± error on the distance modulus (absolute magnitude only).

6 DISCUSSION

We obtained NIR (*H* and *Ks* band) images of 62 ULXs in 37 nearby galaxies to search for NIR counterparts that could be RSG companions. For 17 ULXs, we detected a candidate counterpart in one or more images. 12 of these have absolute magnitudes that are consistent with those of RSGs (whose absolute magnitudes range from −8 (K0) to −10.5 (M5) in the *K* band, Elias et al. 1985; Drilling & Landolt 2000). One of these, Ho I XMM1, we suspect to be a background active galactic nucleus (AGN; see Section 6.2); we cannot exclude the possibility that other RSG candidates are also background AGN. The remaining five sources have an absolute magnitude <−11. These brightest sources are not likely to be single stars. They could be background AGN or (young) stellar clusters; see Section 6.2 for more details on the individual sources.

For the other 45 sources in our sample, we obtained limiting magnitudes. Several of these ULX candidates have known optical counterparts, although in many cases it is not clear what is the source of the optical emission: a companion star or emission from an irradiated accretion disc.

The distribution of absolute magnitudes of the detected counterparts is plotted in Fig. 1. At the faint end, our sample is not complete,

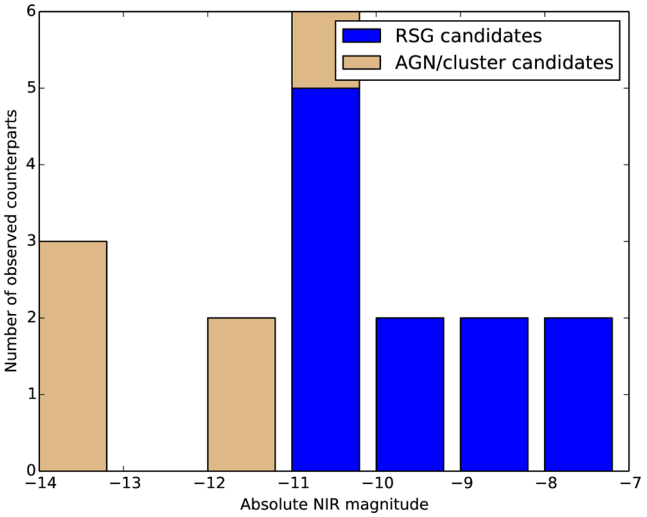

Figure 1. The distribution of absolute magnitudes of the detected candidate counterparts. For ULXs with both *H*- and *Ks*-band counterparts only the *H*-band magnitude is included.

Downloaded from http://mnras.oxfordjournals.org/ at Durham University Library on July 8, 2014

so nothing can be inferred from the shape of the distribution. At absolute magnitudes below −11, however, we expect to detect nearly all NIR sources. This is also the magnitude that the brightest single RSGs can reach. The sharp drop in the number of detections below that magnitude therefore seems to imply that we do detect a population of possible single stars, the more so because the brightest sources are either confirmed background AGN or strong candidates to be background AGN or star clusters.

The fact that only a fraction of the ULXs has a bright NIR counterpart could reflect a difference between systems with blue supergiant or Wolf–Rayet donor stars and systems with RSG donor stars. The ratio of blue to RSGs is not well known, and the ratio of non-detections to candidate RSG detections in our sample of $45/11 \approx 4.1$ is consistent with what has been observed (Langer & Maeder 1995). Alternatively, the systems where we detected NIR counterparts might have larger accretion discs than the ones without an NIR detection, causing the excess NIR radiation. This scenario would suggest that the black holes in those ULXs have larger Roche lobes, either because they have a higher mass than the black holes in systems without bright NIR counterparts (assuming they have the same companion stars), or because the initial separation between the black hole and companion star was larger and hence, when the contact phase starts, the companion star is more evolved and both the disc and star are larger.

Another possibility is that the infrared radiation originates from a jet. We investigated this scenario for the only ULX in our sample with an NIR counterpart and an observed radio jet: Holmberg II X-1. We find that the counterpart that we detected is ∼6 mag brighter than what we would expect as contribution from the jet if it has a steep spectrum ($\alpha \approx -0.8$, for $S_\nu \propto \nu^\alpha$, as is common for jets from X-ray binaries accreting at high rates (Fender, Homan & Belloni 2009). If the radio emission is due to a steady jet with a flat spectrum ($\alpha = 0$) it would contribute significantly to the NIR emission, but such jets usually appear in the low/hard state (see Section 6.1 – Holmberg II X-1). Finding a ULX in the low/hard state would be strong evidence for an IMBH. In principle, the X-ray spectra of ULXs in the 'ultraluminous' state (showing a soft excess and a rollover in the spectrum above 3 keV, Gladstone et al. 2009) can be interpreted as a low/hard state with X-ray reflection from an ionized disc (Caballero-García & Fabian 2010). However, this interpretation has been ruled out at least for a number of ULXs (e.g. Bachetti et al. 2013) by observations of their hard X-ray spectra with *NuSTAR* (Harrison et al. 2013), and thus far only HLX-1 has been observed in a state that is reminiscent of the low/hard state (Godet et al. 2009).

In Sections 6.1 and 6.2, we discuss the systems with NIR counterparts in more detail.

6.1 Candidate red supergiants

For 12 sources in our sample, we have detected an NIR counterpart with an absolute magnitude consistent with that of an RSG, one of which we suspect to be a background AGN. The NIR images of the remaining 11 RSG candidates are shown in Fig. 2.

Two sources, J080157+504339 in NGC 2500 and Holmberg II X-1, were observed twice in the *Ks* band, J080157+504339 on 2012 January 1 and January 7 and Holmberg II X-1 on 2012 January 5 and 2013 January 27. In both cases, the source brightness was consistent with being the same at the two epochs.

We have measured $H - K$ colours for 4 of the 11 RSG candidates (J022721+333500 and J022727+333443 in NGC 925, J024323+372038 in NGC 1058 and Holmberg II X-1). The measured values are 0.7 ± 0.3, 0.6 ± 0.3, 1.1 ± 0.5 and 1.3 ± 0.3, respectively. With the caveat that the images in the two bands were taken several months apart (although if the NIR emission is indeed dominated by an RSG, it is not expected to vary significantly), and the errors are large, these are rather high values for RSGs, whose $H - K$ colours range from 0 to 0.3 (Cox 2000). It is unlikely that the red colours are caused by extinction, because the hydrogen column densities needed for this would be too high. For example, to cause a reddening of $H - K = 0.5$, one needs an extinction in the V band $A_V \approx 8$ (based on relative extinctions from Cardelli, Clayton & Mathis 1989). This corresponds to a hydrogen column density $N_H \approx 1.8 \times 10^{22}$ cm^{-2} (Güver & Özel 2009). Although hydrogen column densities of ULXs can vary significantly, they do not usually reach such values. For instance for Holmberg II X-1, the hydrogen column density inferred from the X-ray spectrum is $N_H = 3.7 \times 10^{21}$ cm^{-2} (Kaaret, Ward & Zezas 2004). The ULX with one of the highest absorption columns known, M82 X-1, has $N_H = 1.12 \times 10^{22}$ cm^{-2} (Kaaret, Simet & Lang 2006), still not nearly enough to account for a reddening of $H - K > 0.5$. Other possible mechanisms that could cause the red $H - K$ colours include a contribution from jets, although that seems unlikely based on the expected NIR contribution from the jet in Holmberg II X-1. It is also possible that there are strong (nebular) emission lines present that cause the red colours if those are stronger in the K than in the H band.

J004722-252051

This ULX candidate in NGC 253 has an X-ray luminosity of $(2.9 \pm 0.12) \times 10^{39}$ erg s^{-1} (90 per cent confidence). The X-ray source is variable on short time-scales (Barnard 2010, their ULX1). We detected a counterpart to this X-ray source in our *Ks*-band image with an absolute magnitude of $Ks = -10.5 \pm 0.03 \pm 0.5 \pm 0.10$ (the errors are the statistical error on the magnitude, the error on the zero-point of the image and the error on the distance modulus, respectively). This absolute magnitude is consistent with that of an M-type supergiant; spectroscopic observations may shed more light on the nature of this source.

J022721+333500

We detected the counterpart to this ULX candidate in NGC 925 in both the H and the *Ks* band, with absolute magnitudes $H = -10.6 \pm 0.03 \pm 0.2 \pm 0.4$ and $Ks = -11.3 \pm 0.03 \pm 0.2 \pm 0.4$. The source is rather bright for a single star, but within the uncertainties the absolute magnitudes are still consistent with an M-type supergiant. The counterpart is extended in both the *H*- and *Ks*-band image (see Fig. 2). If it indeed consists of two sources of about equal brightness, one of them could be the true counterpart of the ULX and that single source would be fainter than the absolute magnitudes that we find for the combined sources.

J022727+333443

The second ULX candidate in NGC 925 has a higher X-ray luminosity than most sources in our sample, reaching $\sim 2.5 \times 10^{40}$ erg s^{-1} (Swartz et al. 2011). A candidate counterpart is detected in both our *H*- and *Ks*-band image, with absolute magnitudes of $Ks = -9.8 \pm 0.08 \pm 0.2 \pm 0.4$ and $H = -9.2 \pm 0.08 \pm 0.2 \pm 0.4$. These magnitudes are consistent with those of an RSG.

Downloaded from http://mnras.oxfordjournals.org/ at Durham University Library on July 8, 2014

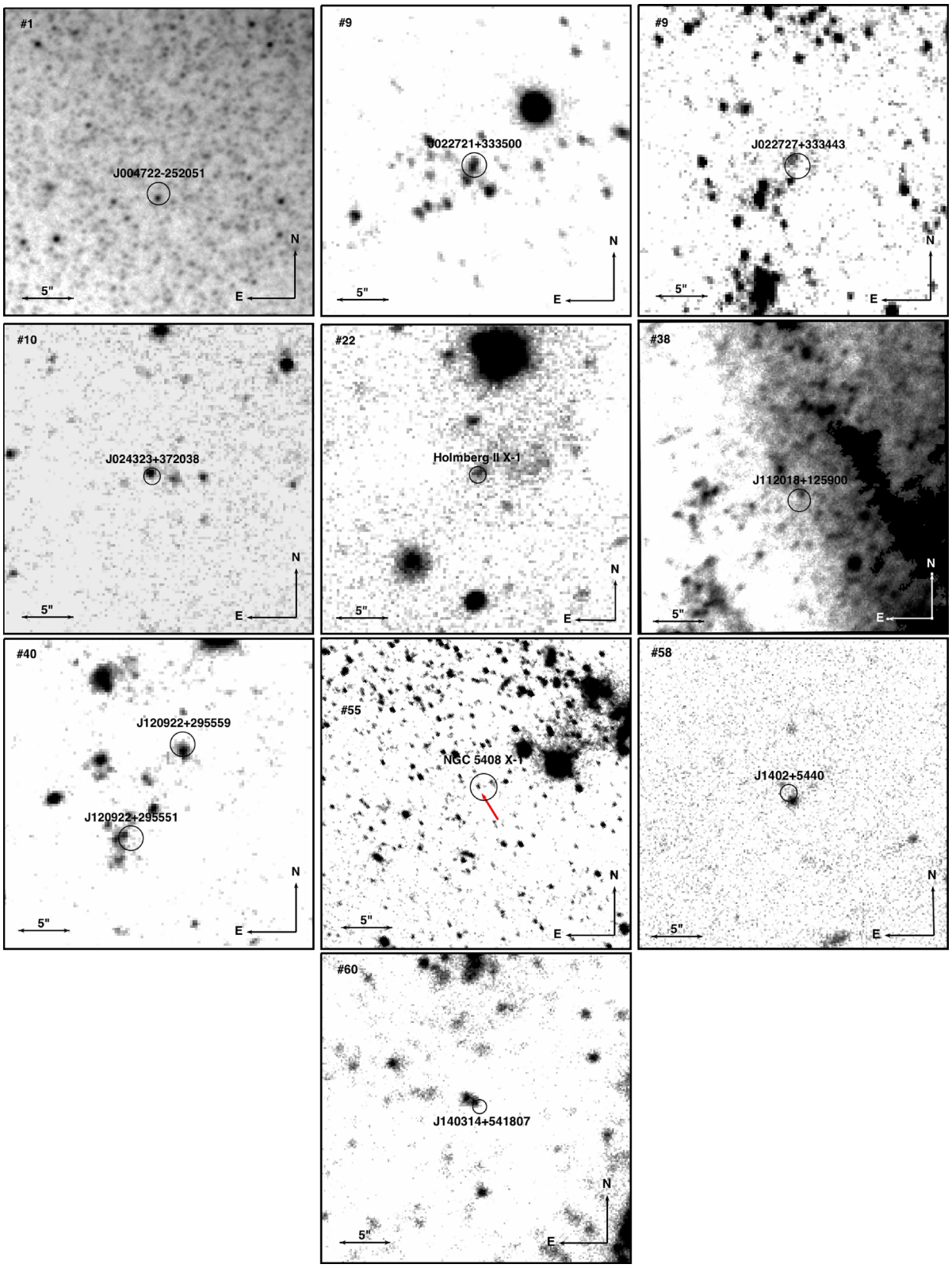

Figure 2. 0.5 arcmin × 0.5 arcmin finder charts of all ULXs with a candidate counterpart that could be a RSG. The black circles are the 95 per cent confidence error circles around the positions of the ULXs. The numbers in the upper-left corners refer to the image numbers in Table 4.

J024323+372038

This ULX candidate is located in the outskirts of NGC 1058. It has a candidate counterpart with absolute magnitudes of $Ks = -10.1 \pm 0.06 \pm 0.4 \pm 0.4$ and $H = -9.0 \pm 0.2 \pm 0.3 \pm 0.4$, if it is at the distance to NGC 1058. These absolute magnitudes are compatible with the source being a red supergiant. Because the ULX candidate is not located in a spiral arm and no signs of recent

Downloaded from http://mnras.oxfordjournals.org/ at Durham University Library on July 8, 2014

star formation are visible in the NIR images, we have to take into account the possibility that this is a foreground star or background AGN. Spectroscopic observations are necessary to determine the true distance to this source.

Holmberg II X-1

Holmberg II X-1 is a ULX with an X-ray luminosity of $\sim 10^{40}$ erg s^{-1}. It has an optical counterpart with a *V*-band magnitude of 21.86 ± 0.09 surrounded by an ionized nebula (Pakull & Mirioni 2002; Kaaret et al. 2004; Moon et al. 2011) and its UV and optical emission are best fitted by an irradiated disc model (Tao et al. 2012). The source has also been detected in radio observations, and recently Cseh et al. (2014) reported the discovery of recurrent radio jets from the ULX. Taking the flux density of the radio core and the spectral index of $\alpha = -0.8 \pm 0.2$ reported by Cseh et al. (2014), the NIR emission expected from the central component has an apparent *Ks*-band magnitude of ∼25.3, 6 mag fainter than the counterpart that we detected. This spectrum is consistent with optically thin synchrotron emission, as expected for intermittent jets occurring at high accretion rates (Fender et al. 2009). If we assume a flat spectrum (expected for steady jets in the low/hard state) then the *Ks*-band magnitude would be ∼16.5, 3.5 mag brighter than what we detect. The spectral index needed to explain the *Ks*-band emission is $\alpha \approx -0.25$. Note that the X-ray spectrum of Holmberg II X-1 indicates that it is not in the low/hard state but instead in an 'ultraluminous' state, possibly accreting above the Eddington limit (e.g. Gladstone, Roberts & Done 2009; Sutton, Roberts & Middleton 2013). It is therefore unlikely that the radio emission is due to a steady jet with a flat spectrum and we do not expect jet emission to contribute significantly to the NIR light.

The absolute magnitude of the counterpart of $Ks = -8.35 \pm 0.08 \pm 0.10 \pm 0.03$, $H = -7.1 \pm 0.3 \pm 0.10 \pm 0.03$ indicates that the infrared excess might be due to an RSG companion. It could also be related to the nebula surrounding the ULX.

J112018+125900

J112018+125900 is a ULX candidate located on the edge of a spiral arm in NGC 3627. Its absolute *Ks*-band magnitude of $-9.1 \pm 1.9 \pm 0.7 \pm 0.4$ puts it in the magnitude range of RSGs, but its apparent magnitude ($20.6 \pm 1.9 \pm 0.7$ in the *Ks*-band) and its location in a crowded region will make it difficult to observe it spectroscopically with current instrumentation.

J120922+295551

This ULX candidate in NGC 4136 was detected by the ROSAT High Resolution Imager at 2.5×10^{39} erg s^{-1} (Lira, Lawrence & Johnson 2000), and subsequently at much lower luminosity in a *Chandra* observation by Roberts et al. (2004). We detected a counterpart with an absolute *H*-band magnitude of $-10.78 \pm 0.03 \pm 0.10 \pm 0.4$. Within the uncertainties this is compatible with an M-type RSG companion.

J120922+295559

The second ULX candidate in NGC 4136 was discovered by Roberts et al. (2004) in a *Chandra* observation, at ∼11 arcsec from J120922+295551 with a maximum unabsorbed X-ray luminosity of 2.6×10^{39} erg s^{-1}. Its NIR counterpart has an absolute *H*-band magnitude of $-10.75 \pm 0.03 \pm 0.10 \pm 0.4$. Within the uncertainties this is compatible with an M-type RSG companion.

NGC 5408 X-1

Lang et al. (2007) discovered an optical counterpart to this ULX in *Hubble Space Telescope* (*HST*) images with a *V*- and *I*-band magnitude of 22.4. The counterpart has also been studied by Grisé et al. (2012), who discovered it in 6 *HST* filters from the near UV to the NIR. They find that the flux of the source drops continuously with increasing wavelength to $\sim 0.13 \times 10^{-18}$ erg s^{-1} cm^{-2} Å^{-1} in the *H* band and concluded that the companion star was either a blue (O- or B-type) supergiant or the optical emission was dominated by the accretion disc. Optical spectra obtained with the VLT show a blue continuum superimposed with emission lines from the surrounding nebula (Kaaret & Corbel 2009; Cseh et al. 2011).

Radio emission from the nebula has also been detected by Lang et al. (2007); since the emission is resolved in their VLA images, they conclude that it cannot originate in a relativistic jet. The flux density and spectral index of this radio source are similar to those of the compact radio jet in Holmberg II X-1, so assuming that the spectrum continues into the NIR we would expect a similar magnitude for NGC 5408 X-1 of *Ks* ∼25, five magnitudes fainter than what we detect.

The error circle in our image actually contains two sources, but comparison with the *HST* image of Lang et al. (2007) shows that the most Eastern source (indicated with an arrow in Fig. 2) is the counterpart. This source has an apparent *Ks*-band magnitude of $20.3 \pm 0.13 \pm 0.2$. At the distance of NGC 5408 this corresponds to an absolute *Ks*-band magnitude of $-8.1 \pm 0.13 \pm 0.2 \pm 0.8$. Interestingly, this corresponds to a higher flux ($\sim 0.3 \times 10^{-18}$ erg s^{-1} cm^{-2} Å^{-1}) than Grisé et al. (2012) measured in the *H* band, while none of their models predict an increase in flux towards the *Ks* band. It is possible that this excess infrared radiation is emitted by the companion star, while most of the optical emission originates from the disc. However, RSGs typically have $H - K \approx 0$, while for this source we find $H - K \approx 2$ (based on the *H*-band magnitude reported by Grisé et al. 2012). Since the *Ks*-band image was not taken simultaneously with the optical and *H*-band data, variability of the source is also a possible explanation.

J1402+5440

One of the four ULX candidates that we observed in M101, this source has a reported X-ray luminosity of 2.4×10^{39} erg s^{-1} (Swartz et al. 2011). The counterpart that we detected in our *H*-band image has an absolute magnitude of $-9.7 \pm 0.04 \pm 0.2 \pm 0.05$. This places it in the magnitude range of RSGs.

J140314+541807

J140314+541807 is another ULX in M101 with an X-ray luminosity of 2.9×10^{39} erg s^{-1} as reported by Winter et al. (2006). We detected a counterpart in the *H* band with an absolute magnitude of $-10.69 \pm 0.03 \pm 0.10 \pm 0.05$. Within the uncertainties this is compatible with an M-type RSG companion.

6.2 Candidate star clusters and background AGN

Five of the candidate counterparts that we discovered have absolute magnitudes that are incompatible with them being single stars.

Downloaded from http://mnras.oxfordjournals.org/ at Durham University Library on July 8, 2014

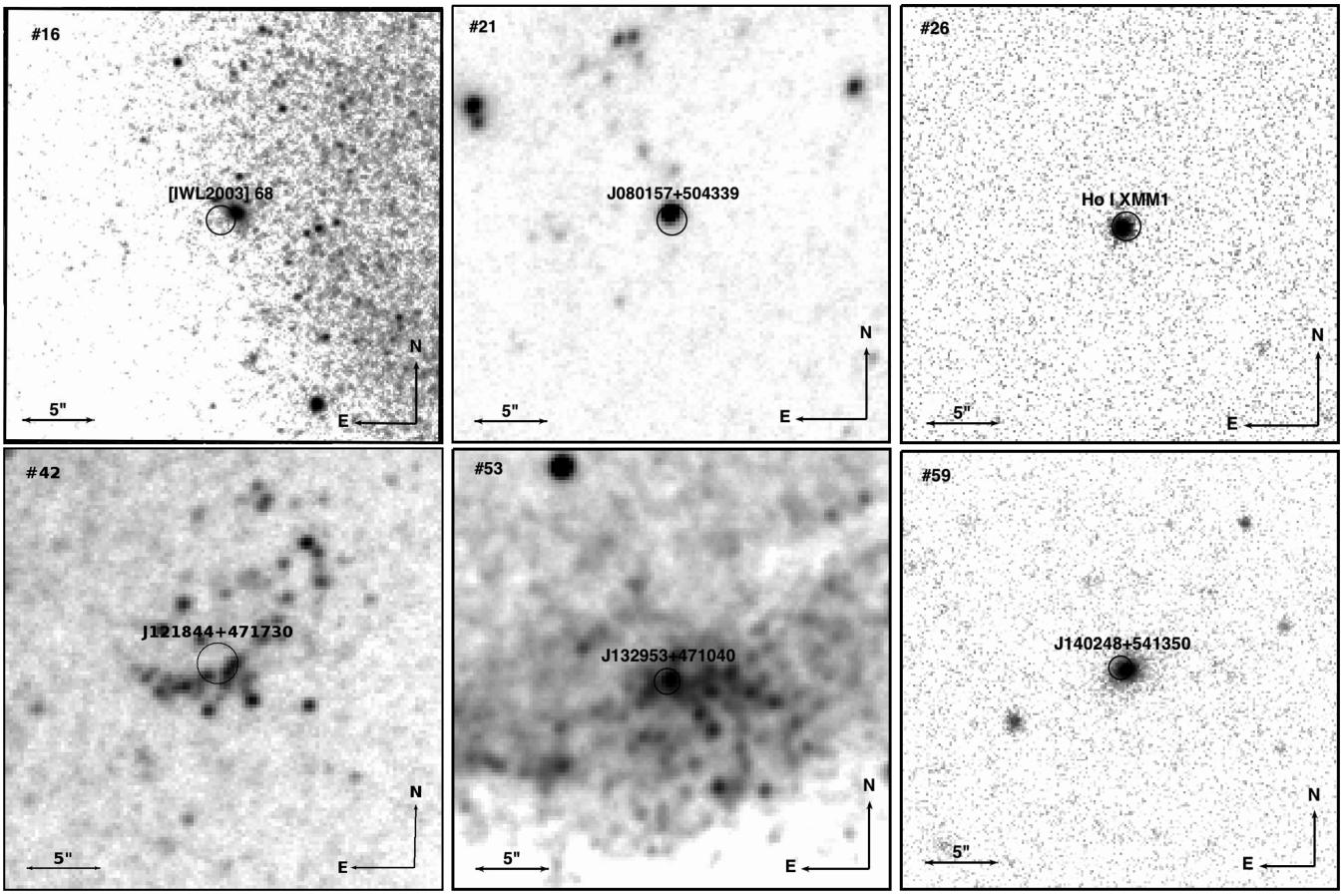

Figure 3. 0.5 arcmin × 0.5 arcmin finder charts of all ULXs with a candidate counterpart that are likely or confirmed background AGN or (young) stellar clusters. The black circles are the 95 per cent confidence error circles around the positions of the ULXs. The numbers in the upper-left corners refer to the image numbers in Table 4.

Some of these can be classified as background AGN; others might be bona fide ULXs located in stellar clusters (cf. Voss et al. 2011; Jonker et al. 2012). Additionally, two of the ULX candidates near Holmberg I are likely not real ULXs but background AGN. We discuss these sources in more detail below; the NIR images of these sources are shown in Fig. 3.

[IWL2003] 68

The absolute magnitude of the *Ks*-band counterpart to this ULX candidate in NGC 1637 is $-13.7 \pm 0.005 \pm 0.5 \pm 0.4$. This is much brighter than a single RSG. The source is resolved in our *Ks*-band image. The counterpart has also been detected in *HST* images of the galaxy by Immler et al. (2003), who report apparent magnitudes $m_V \sim 22.8$ and $m_I \sim 21.1$ and a full width at half-maximum (FWHM) of 0.45 arcsec, more than twice as large as the size of the point sources in the image. At the distance to NGC 1637 this corresponds to a physical size of ∼25 pc. The counterpart could be a star cluster in NGC 1637, or a background galaxy containing an AGN.

J080157+504339

This ULX candidate, situated in NGC 2500, has a bright counterpart that we detected in two *Ks*-band observations at an absolute magnitude of $-14.3 \pm 0.002 \pm 0.2 \pm 0.4$ and $-14.1 \pm 0.005 \pm 0.15 \pm 0.4$, respectively, if the distance to NGC 2500 is assumed. However, optical spectroscopic observations by Gutiérrez (2013) have shown this source to be a background AGN.

Ho I XMM1

The ULX candidate Ho I XMM1 is situated at 5 arcmin from the centre of the dwarf irregular galaxy Holmberg I. The galaxy has a diameter (semimajor axis) of 3.6 arcmin (Gil de Paz et al. 2007); the X-ray source is thus located outside the galaxy itself. The *H*-band counterpart that we detected has an absolute magnitude of $-10.14 \pm 0.01 \pm 0.10 \pm 0.03$. This in itself does not exclude the possibility that the counterpart is an RSG. However, it has also been detected by the *Wide-Field Infrared Survey Explorer* (*WISE*) and its colours in the WISE bands are [3.4]-[4.6] = 0.8, [4.6]-[12] = 2.5, placing it firmly among the AGN in *WISE* colour–colour diagrams (cf. Stern et al. 2005; D'Abrusco et al. 2012). Thus, it is likely that this ULX candidate is a background AGN like J080157+504339 in NGC 2500.

J0940+7106

J0940+7106 is another ULX candidate 5 arcmin from the centre of Holmberg I. It does not have a counterpart within the 95 per cent confidence error circle of 1.1 arcsec, but a single NIR point source is located just outside it. This NIR source was also detected by *WISE*. Its colours are [3.4]-[4.6] = 1.35, [4.6]-[12] = 2.4, which place the

Downloaded from http://mnras.oxfordjournals.org/ at Durham University Library on July 8, 2014

source among the Seyfert galaxies in the diagram of D'Abrusco et al. (2012). Therefore, we expect that the X-ray source and the NIR source are related, and that this ULX candidate is also in fact a background AGN.

J121844+471730

This ULX candidate in NGC 4258 is located in the centre of a cluster of stars. The counterpart has an absolute *H*-band magnitude of $-11.50 \pm 0.02 \pm 0.1 \pm 0.02$ and is thus too bright to be a single star.

J132953+471040

The counterpart to J132953+471040 in M51 has an absolute *H*-band magnitude of $-13.88 \pm 0.02 \pm 0.10 \pm 0.2$. Comparing to the *HST* image of Terashima et al. (2006), we find that this source is at the centre of the star cluster in which the ULX is located. Even in the higher resolution *HST* image this source is unresolved, although extended, and it is not possible to distinguish single stars.

J140248+541350

This ULX candidate in M101 is associated with an optical counterpart in the Sloan Digital Sky Survey (SDSS) catalogue (Pineau et al. 2011). The SDSS source is classified as a galaxy in all Sloan filters except the u' band. We also detected the counterpart in our *H*-band image, where it is clearly extended (see Fig. 3). This source is likely to be a background galaxy harbouring an AGN.

6.3 Non-detections of sources with known optical counterparts

Several ULX candidates in our sample have known optical counterparts, and optical spectra are available for a few. Some of these we did detect in our NIR images (see Sections 5.1 and 5.2), but the majority were not detected by us. Ptak et al. (2006), Tao et al. (2011) and Gladstone et al. (2013) found (sometimes multiple) candidate optical counterparts in archival *HST* data for 11 ULXs that we do not detect in our images (J004742−251501, J0318−6629, J034555+680455, J034615+681112, J073625+653539, NGC 3031 ULX1, Holmberg IX X-1, J112020+125846, IXO 53, J123551+27561, J132519−430312 and J132938+582506). Optical spectra are available for Holmberg IX X-1, J132938+582506 in NGC 5204 (both in Roberts et al. 2011) and J140332+542103 in M101 (Liu et al. 2013).

The *V*-band apparent magnitudes for these counterparts lie between 22 and 25. Holmberg II X-1 and NGC 5408 X-1, the only two RSG candidates that we detect in the NIR that have also been detected in the optical, have values for $V-K \sim 2.1-2.5$ (not taking into account possible variability). Typical $V-K$ values for RSGs range from ∼2 to 4, but in ULXs there will also be a contribution from the accretion disc to the optical light, which lowers $V-K$. For the ULXs with *V*-band magnitude up to ∼22, we can state that they have $V-K$ closer to 0, because otherwise we would have detected them in our NIR images. Indeed, for Holmberg IX X-1 (with a *V* −band magnitude of ∼22.8, Grisé, Pakull & Motch 2006) there is also an *HST H*-band observation in which the counterpart is detected at a magnitude of 22.56 (Grisé et al., in preparation). These $V-K$ values are in line with what would be expected for early-type companion stars (Elias et al. 1985). The ULXs with $V \approx 23-24$ we would not have detected in our NIR images if they have $V-K \approx 2.5$, but we can exclude that they have $V-K$ values that are even higher. The ULXs with the very faintest optical counterparts, with $V \gtrsim 25$, we could not detect even if they had $V-K \approx 4$.

7 CONCLUSIONS

We have performed the first systematic search for near-infrared counterparts to nearby ULXs. We observed 62 ULXs in the *H*- and/or *Ks*-band and detected candidate counterparts for 17 of them. For the other 45 ULXs, we determined limiting magnitudes. Of the 17 ULXs with NIR counterparts, 11 had no previously reported optical or NIR counterpart. We detected 11 candidate counterparts with absolute magnitudes that are consistent with them being single RSGs. Two of these (Holmberg II X-1 and NGC 5408 X-1) also have known optical counterparts. Holmberg II X-1 has a radio jet, but the NIR emission that we detect is 6 mag brighter than the emission expected from the jet. In NGC 5408 X-1, we detected excess *Ks*-band emission compared to the models tested by Grisé et al. (2012). This excess infrared radiation could be emitted by the companion star, while most of the optical emission originates from the disc. However, this would not explain the large value for $H-K$ in this ULX. It is also possible that the source is variable.

Six counterparts are too bright to be single stars and in some cases extended; they are likely star clusters or background galaxies.

The fact that we detect only a fraction of the ULXs in our NIR images points towards differences between ULX systems: the systems that show relatively strong NIR emission might have larger accretion discs than the ones that do not, or there may be strong nebular lines present that are absent in other sources. Alternatively, these systems may contain RSG donor stars that are intrinsically bright in the NIR. If the NIR emission indeed originates from a late-type donor star, these systems are excellent candidates for future spectroscopic studies to find dynamical masses for their black holes.

ACKNOWLEDGEMENTS

EK thanks Mischa Schirmer for his help with the data-reduction software THELI. We thank the anonymous referee for their comments that helped improve the paper. TPR's contribution to this paper was funded as part of STFC consolidated grant ST/K000861/1. Based on observations collected at the European Southern Observatory, Chile, programmes 089.D-0663(A) and 090.D-0417(A). The William Hershel Telescope is operated on the island of La Palma by the Isaac Newton Group in the Spanish Observatorio del Roque de los Muchachos of the Instituto de Astrofisica de Canarias. Observations reported here were obtained at the MMT Observatory, a joint facility of the Smithsonian Institution and the University of Arizona.

REFERENCES

Bachetti M. et al., 2013, ApJ, 778, 163
Barnard R., 2010, MNRAS, 404, 42
Begelman M. C., 2002, ApJ, 568, L97
Belczynski K., Bulik T., Fryer C. L., Ruiter A., Valsecchi F., Vink J. S., Hurley J. R., 2010, ApJ, 714, 1217
Bertin E., 2006, in Gabriel C., Arviset C., Ponz D., Enrique S., eds, ASP Conf. Ser. Vol. 351, Astronomical Data Analysis Software and Systems XV. Astron. Soc. Pac., San Francisco, p. 112
Bertin E., Arnouts S., 1996, A&AS, 117, 393

Downloaded from http://mnras.oxfordjournals.org/ at Durham University Library on July 8, 2014

Bertin E., Mellier Y., Radovich M., Missonnier G., Didelon P., Morin B., 2002, in Bohlender D. A., Durand D., Handley T. H., eds, ASP Conf. Ser. Vol. 281, Astronomical Data Analysis Software and Systems XI. Astron. Soc. Pac., San Francisco, p. 228
Caballero-García M. D., Fabian A. C., 2010, MNRAS, 402, 2559
Cardelli J. A., Clayton G. C., Mathis J. S., 1989, ApJ, 345, 245
Chattopadhyay A. K., Chattopadhyay T., Davoust E., Mondal S., Sharina M., 2009, ApJ, 705, 1533
Copperwheat C., Cropper M., Soria R., Wu K., 2005, MNRAS, 362, 79
Copperwheat C., Cropper M., Soria R., Wu K., 2007, MNRAS, 376, 1407
Cox A. N., 2000, Allen's Astrophysical Quantities. Springer-Verlag, Berlin
Cseh D., Grisé F., Corbel S., Kaaret P., 2011, ApJ, 728, L5
Cseh D., Grisé F., Kaaret P., Corbel S., Scaringi S., Groot P., Falcke H., Körding E., 2013, MNRAS, 435, 2896
Cseh D. et al., 2014, MNRAS, 439, L1
D'Abrusco R., Massaro F., Ajello M., Grindlay J. E., Smith H. A., Tosti G., 2012, ApJ, 748, 68
Dalcanton J. J. et al., 2009, ApJS, 183, 67
Drilling J. S., Landolt A. U., 2000, in Cox A., ed., Normal Stars, Springer-Verlag, Berlin, p. 381
Drozdovsky I. O., Karachentsev I. D., 2000, A&AS, 142, 425
Durrell P. R., Sarajedini A., Chandar R., 2010, ApJ, 718, 1118
Elias J. H., Frogel J. A., Humphreys R. M., 1985, ApJS, 57, 91
Fabbiano G., Zezas A., Murray S. S., 2001, ApJ, 554, 1035
Farrell S. A., Webb N. A., Barret D., Godet O., Rodrigues J. M., 2009, Nature, 460, 73
Fender R. P., Homan J., Belloni T. M., 2009, MNRAS, 396, 1370
Feng H., Kaaret P., 2008, ApJ, 675, 1067
Feng H., Soria R., 2011, New Astron. Rev., 55, 166
Fruscione A. et al., 2006, in Silva D. R., Doxsey R. E., eds, Proc. SPIE Conf. Ser., Vol. 6270, Observatory Operations: Strategies, Processes, and Systems. SPIE, Bellingham, p. 62701V
Gao Y., Wang Q. D., Appleton P. N., Lucas R. A., 2003, ApJ, 596, L171
Gil de Paz A. et al., 2007, ApJS, 173, 185
Gladstone J. C., Roberts T. P., Done C., 2009, MNRAS, 397, 1836
Gladstone J. C., Copperwheat C., Heinke C. O., Roberts T. P., Cartwright T. F., Levan A. J., Goad M. R., 2013, ApJS, 206, 14
Gliozzi M., Satyapal S., Eracleous M., Titarchuk L., Cheung C. C., 2009, ApJ, 700, 1759
Godet O., Barret D., Webb N. A., Farrell S. A., Gehrels N., 2009, ApJ, 705, L109
Grisé F., Pakull M. W., Motch C., 2006, in Meurs E. J. A., Fabbiano G., eds, Proc. IAU Symp. 230, Populations of High Energy Sources in Galaxies. Cambridge Univ. Press, Cambridge, p. 302
Grisé F., Kaaret P., Corbel S., Feng H., Cseh D., Tao L., 2012, ApJ, 745, 123
Gutiérrez C. M., 2013, A&A, 549, A81
Güver T., Özel F., 2009, MNRAS, 400, 2050
Harrison F. A. et al., 2013, ApJ, 770, 103
Herrmann K. A., Ciardullo R., Feldmeier J. J., Vinciguerra M., 2008, ApJ, 683, 630
Humphreys E. M. L., Reid M. J., Greenhill L. J., Moran J. M., Argon A. L., 2008, ApJ, 672, 800
Immler S., Wang Q. D., Leonard D. C., Schlegel E. M., 2003, ApJ, 595, 727
Jacobs B. A., Rizzi L., Tully R. B., Shaya E. J., Makarov D. I., Makarova L., 2009, AJ, 138, 332
Jonker P. G. et al., 2012, ApJ, 758, 28
Kaaret P., Corbel S., 2009, ApJ, 697, 950
Kaaret P., Corbel S., Prestwich A. H., Zezas A., 2003, Science, 299, 365
Kaaret P., Ward M. J., Zezas A., 2004, MNRAS, 351, L83
Kaaret P., Simet M. G., Lang C. C., 2006, ApJ, 646, 174
Karachentsev I. D. et al., 2003, A&A, 398, 467
King A. R., Davies M. B., Ward M. J., Fabbiano G., Elvis M., 2001, ApJ, 552, L109
Kraft R. P., Kregenow J. M., Forman W. R., Jones C., Murray S. S., 2001, ApJ, 560, 675
Lang C. C., Kaaret P., Corbel S., Mercer A., 2007, ApJ, 666, 79
Langer N., Maeder A., 1995, A&A, 295, 685
Lin D., Webb N. A., Barret D., 2012, ApJ, 756, 27
Lira P., Lawrence A., Johnson R. A., 2000, MNRAS, 319, 17
Liu J., 2011, ApJS, 192, 10
Liu J.-F., Bregman J. N., 2005, ApJS, 157, 59
Liu Q. Z., Mirabel I. F., 2005, A&A, 429, 1125
Liu J.-F., Bregman J. N., Seitzer P., 2002, ApJ, 580, L31
Liu J., Orosz J., Bregman J. N., 2012, ApJ, 745, 89
Liu J.-F., Bregman J. N., Bai Y., Justham S., Crowther P., 2013, Nature, 503, 500
McQuinn K. B. W. et al., 2010, ApJ, 721, 297
Mineo S., Gilfanov M., Sunyaev R., 2012, MNRAS, 419, 2095
Monet D. G. et al., 2003, AJ, 125, 984
Moon D.-S., Eikenberry S. S., Wasserman I. M., 2003, ApJ, 586, 1280
Moon D.-S., Harrison F. A., Cenko S. B., Shariff J. A., 2011, ApJ, 731, L32
Moorwood A. et al., 1998, The Messenger, 94, 7
Olivares E. F. et al., 2010, ApJ, 715, 833
Pakull M. W., Mirioni L., 2002, preprint (arXiv:0202488)
Patruno A., Zampieri L., 2008, MNRAS, 386, 543
Pineau F.-X., Motch C., Carrera F., Della Ceca R., Derrière S., Michel L., Schwope A., Watson M. G., 2011, A&A, 527, A126
Poznanski D. et al., 2009, ApJ, 694, 1067
Ptak A., Colbert E., van der Marel R. P., Roye E., Heckman T., Towne B., 2006, ApJS, 166, 154
Roberts T. P., Goad M. R., Ward M. J., Warwick R. S., O'Brien P. T., Lira P., Hands A. D. P., 2001, MNRAS, 325, L7
Roberts T. P., Warwick R. S., Ward M. J., Murray S. S., 2002, MNRAS, 337, 677
Roberts T. P., Warwick R. S., Ward M. J., Goad M. R., 2004, MNRAS, 349, 1193
Roberts T. P., Gladstone J. C., Goulding A. D., Swinbank A. M., Ward M. J., Goad M. R., Levan A. J., 2011, Astron. Nachr., 332, 398
Roeser S., Demleitner M., Schilbach E., 2010, AJ, 139, 2440
Schirmer M., 2013, ApJS, 209, 21
Shappee B. J., Stanek K. Z., 2011, ApJ, 733, 124
Sivakoff G. R. et al., 2008, ApJ, 677, L27
Skrutskie M. F. et al., 2006, AJ, 131, 1163
Soria R., Kuntz K. D., Winkler P. F., Blair W. P., Long K. S., Plucinsky P. P., Whitmore B. C., 2012, ApJ, 750, 152
Springob C. M., Masters K. L., Haynes M. P., Giovanelli R., Marinoni C., 2009, ApJS, 182, 474
Steeghs D., McClintock J. E., Parsons S. G., Reid M. J., Littlefair S., Dhillon V. S., 2013, ApJ, 768, 185
Stern D. et al., 2005, ApJ, 631, 163
Sutton A. D., Roberts T. P., Middleton M. J., 2013, MNRAS, 435, 1758
Swartz D. A., Ghosh K. K., Tennant A. F., Wu K., 2004, ApJS, 154, 519
Swartz D. A., Tennant A. F., Soria R., 2009, ApJ, 703, 159
Swartz D. A., Soria R., Tennant A. F., Yukita M., 2011, ApJ, 741, 49
Tao L., Feng H., Grisé F., Kaaret P., 2011, ApJ, 737, 81
Tao L., Kaaret P., Feng H., Grisé F., 2012, ApJ, 750, 110
Terashima Y., Wilson A. S., 2004, ApJ, 601, 735
Terashima Y., Inoue H., Wilson A. S., 2006, ApJ, 645, 264
Theureau G., Hanski M. O., Coudreau N., Hallet N., Martin J.-M., 2007, A&A, 465, 71
Tonry J. L., Dressler A., Blakeslee J. P., Ajhar E. A., Fletcher A. B., Luppino G. A., Metzger M. R., Moore C. B., 2001, ApJ, 546, 681
Tully R. B., 1988, Nearby Galaxies Catalog. Cambridge Univ. Press, Cambridge
Tully R. B., Rizzi L., Shaya E. J., Courtois H. M., Makarov D. I., Jacobs B. A., 2009, AJ, 138, 323
Voss R., Nielsen M. T. B., Nelemans G., Fraser M., Smartt S. J., 2011, MNRAS, 418, L124
Walton D. J., Roberts T. P., Mateos S., Heard V., 2011, MNRAS, 416, 1844
Willick J. A., Courteau S., Faber S. M., Burstein D., Dekel A., Strauss M. A., 1997, ApJS, 109, 333
Winter L. M., Mushotzky R. F., Reynolds C. S., 2006, ApJ, 649, 730
Zampieri L., Roberts T. P., 2009, MNRAS, 400, 677

This paper has been typeset from a TEX/LATEX file prepared by the author.

Downloaded from http://mnras.oxfordjournals.org/ at Durham University Library on July 8, 2014